Chapter 9

OPTICAL AND RADAR TECHNIQUES APPLIED TO CHEMICAL RELEASE "ACTIVE EXPERIMENTS" IN THE IONOSPHERE/THERMOSPHERE SYSTEM

Michael Mendillo, Jeffrey Baumgardner and Peter J. Sultan
Center for Space Physics
Boston University
Boston, MA 02215 USA

I. INTRODUCTION TO ACTIVE EXPERIMENTS

I.1 Background.

The term "Active Experiments" refers to a relatively new class of space physics experimentation in which a known perturbation is applied to a natural system in order to study its characteristics through observations and analysis of the induced effects. Such techniques have been applied to the Earth's thermosphere/ionosphere, the magnetosphere and solar wind. There are four general types of stresses used as causative agents in active experiments: (1) neutral gas releases, (2) cold plasma injections, (3) ion and electron beams, and (4) electromagnetic wave injections. Areas (1), (2), and (3) can be handled via sounding rocket or satellite-borne payloads, while (4) can utilize either powerful groundbased transmitters or spaceborne injection methods.

Given the relatively modest scientific payloads that can be carried into earth orbit, the spatial extent and temporal duration associated with active experimentation are small and brief in comparison to those associated with natural, solar-terrestrial-type disturbances. For example, chemical release experiments in the ionosphere produce disturbances spanning 10's to 100's of kilometers that last a few minutes to perhaps a few hours. Ionospheric storms, on the other hand, are global in scale and last for days. Similarly, barium plasma injections in the ionosphere or magnetosphere result in observable effects that typically last for periods less than the duration of a substorm ($\sim$ few hours). Ionospheric heating effects generally last as long as the heating is applied, often in the 10's of minutes domain. The end result is that active experiments require a comprehensive set of multi-diagnostic instruments that can handle the small time constants associated with the induced effects. These pose no particular problems for in-situ probes that sample the regions close to the perturbation; sounding rocket and satellite diagnostics routinely provide high data sets. However, when groundbased radars and optical systems are used in active experiments, the normal modes used for sampling geophysical effects must often be modified to cope with the reduced spatial and temporal time scales of active experiments.

In the following sections, we concentrate on the chemical release experiments used in ionospheric investigations, namely, neutral gas and cold plasma injection experiments. For a general overview of all types of active experiments, the reader is referred to the proceedings of several symposia on Active Experiments in Space held in recent year [Burke, 1983; Haerendel and Mendillo, 1988; Mendillo, 1989; and Brenning, 1989].

I.2. Types of Chemical Release Experiments.

Chemically-induced ionospheric modification experiments involve either the enhancement of ambient plasma densities or their depletion. In the former case, the most widely used technique involves the release of barium vapor into the ionosphere [Foppl et al., 1967; Haerendel, 1976]. Barium is an element that is ionized by solar ultraviolet with a time constant of $\sim$ 28 seconds. The Ba^+ ion has bright emission lines at 4554 and 4934Å, with less intense lines at 5854, 6142, and 6497Å. In its neutral state, Ba has a bright emission line at 5535Å. Barium release experiments are conducted under post-sunset or pre-sunrise conditions using geometries required for darkness on the ground (to permit optical observations) but UV illumination in the ionosphere (to permit optical excitation). Under such conditions, observations can be made for 10's of minutes, depending upon the release altitude and ground site locations.

A Ba^+/e^- plasma responds to electrodynamical effects and thus optical observations can be used to trace ambient electric fields associated with ionospheric-magnetospheric coupling, space plasma instabilities, critical ionization velocity (CIV) effects, and many other phenomena. Again, the reader is referred to the special issues quoted above and to the references contained therein.

Strontium (Sr) vapor has been used in conjunction with Ba release experiments (contained as an impurity or "dopant"), or as an independent species released into the ionosphere/thermosphere. Sr has the property of not being readily ionized ($\tau_i \sim 1$ hour), but is excited in its neutral state by sunlight, and thus it can be used to illuminate the evolution of a gas not subject to electrodynamical forces. It can, for example, trace neutral wind patterns or map diffusion processes. The Sr emission line typically observed is at 4607Å; when Sr^+ is formed, observations can be made at 4078Å.

Many Ba^+ and Sr release experiments are not true active experiments in that they do not modify ambient systems, but rather illuminate or trace existing features. The same can be said for releases of other species such as trimethyl aluminum (TMA), cesium, calcium, etc. These experiments do, however, have the common feature with active experiments of offering a short duration, visible light signal that is observed at a wavelength not confused with regular atmospheric emissions. With often very bright lines to observe, a wide variety of techniques can and have been used to record such emissions, ranging from standard film cameras to specialized video and CCD-based digital imaging systems [Heppner et al, 1981; Stenbaek-Nielsen et al., 1984; Wescott et al., 1986].

The second type of chemical release experiment involves the release of molecules that react very rapidly with ambient ionospheric plasma (Mendillo and Forbes, 1982; Bernhardt, 1987a). These highly reactive rapors (e.g., H_2, CO_2, H_2O, SF_6, CF_3Br, $Ni(CO)_4$) modify the ionosphere via recombination chemistry (plasma neutralization) that leaves the ionospheric F-region plasma in a depleted ("ionospheric hole") state. As part of the photo-chemical chains in the modification process, there is emission of light from the oxygen atoms produced by the neutralization of the ambient O^+/e^- plasma. These enhanced airglow lines (typically at 6300, 7774 and 8446Å) can be used to monitor the chemical reactions and neutral dynamics of the system. Recent reviews of the mechanisms, goals and status of neutral gas induced

active experiments have been given by Mendillo (1988) and Bernhardt (1987a).

The diagnostic challenges presented by neutral gas induced effects center on (1) the reduced signal-to-noise levels for a radar probing the remnant plasma in an ionospheric hole and (2) the short duration, sub-visual airglow enhancements at ambient emission wavelengths that accompany the formation of ionospheric holes. These topics are treated separately in the following sections. They have an obvious relevance to plasma enhancement active experiments where stronger signals would require less integration time for radar and imaging systems.

II. Incoherent Scatter Radar Techniques Applied to Active Experiments

II.1. Background

Incoherent scatter radar is one of the more important and useful observational tools for studying the physics of the upper atmosphere [Evans, 1969,1975]. Physically, it is based on the fact that an upwardly propagating radio wave that is higher in frequency than the plasma frequency anywhere along its path will be weakly re-radiated by the free electrons of the ionosphere. This incoherent scatter, or "Thomson" scattering, provides a small but measureable return signal from a probing radar beam. Because of the weakness of the scattered signal, high powered transmitters and large collecting areas are required for adequate detection.

The returned incoherent scatter signal may be analyzed to determine a wide variety of ionospheric parameters. Of principal interest in active experiments are:

N_e - local electron density. N_e is proportional to the area under the curve of the returned spectrum, and is typically observed up to h $\sim$ 1000 km.

V_i - ion sound speed: derived from the overall width of the spectrum, or from the location of the spectral peaks.

T_i - ion temperature: derived from V_i if the ion masses are known.

T_r - ratio of T_e/T_i: derived from the shape of the returned spectrum.

T_e - electron temperature: calculated from T_r, once T_i is determined.

V_d - large-scale drift of the ionospheric plasma: determined from an observed doppler shift of the entire spectrum.

Currents - differential drifts of electrons and ions can be detected from the presence of different heights of the up- and down-shifted spectral wings [Rosenbluth and Rostoker, 1962].

Composition - mixtures of different ions can be inferred from changes in the shape of the returned spectrum [Moorcroft, 1964].

Simultaneous changes in several different parameters can have a complex effect on the spectral signal. However, in the natural ionosphere, changes in individual spectral parameters

occur over a limited altitude range, making it possible to deconvolve individual effects by making reasonable assumptions as to which parameters are changing, and which remain constant. Thus the scattering from each altitude region can be described in terms of changes in only two or three important parameters.

A typical incoherent scatter analysis program determines ionospheric parameters by calculating theoretical spectra which most clearly match the observed spectra. The various physical parameters controlling the spectrum shape are adjusted to provide for the best least-squares fit between theory and data. An approximation of one or more parameters, such as the ion composition or T_e/T_i profile, can often be made so the other parameters can be derived without ambiguity. Traditional incoherent scatter radar analyses often begin by assuming an O^+/e^- plasma of $T_e/T_i = 1$ near the F_2 peak at night. Additionally, one or more parameters can be pre-determined from an additional data source (e.g. obtain f_oF2 from an ionosonde, or include data from measurements of the incoherent scatter plasma line).

Incoherent scatter radar is a unique and ideal diagnostic instrument for the measurement of ionospheric parameters during active experiments. If the antenna is quickly steerable, there is an added flexibility for observations under rapidly changing circumstances (e.g., sudden changes in rocket trajectory). Observations over time can yield an excellent spatial/temporal picture of the changing conditions in the ionosphere during chemical releases.

The first use of a steerable incoherent scatter radar to observe an artificial, short-duration event took place in 1979 when the Millstone Hill Incoherent Scatter Facility (42.62°N, 71.49°W) measured an ionospheric disturbance to the east of the Kennedy Space Center following the launch of NASA's HEAO-C satellite by an Atlas/Centaur rocket [Wand and Mendillo, 1984]. A chemically-induced rapid recombination of F-region plasma caused by the rocket's exhaust cloud of H_2 and H_2O molecules was monitored by the 46 m diameter Millstone Hill radar, and the spatial, temporal, and dynamical morphologies of a large-scale 'ionospheric hole' were observed for the first time. The incoherent scatter studies of the rocket launch effects showed that reliable altitude profiles of electron densities, plasma temperatures and bulk plasma drift speeds can be obtained during active experiments.

During the HEAO-C event, the main difficulties with the observations resulted from the large distance between the perturbation and observation sites. As described in Evans (1969), radar range resolution (ΔS) depends upon pulse duration (Δt) via $\Delta S = \frac{1}{2}c\Delta t$ where c is the speed of light. In order to achieve acceptable signal to noise (S/N) levels for the radar returns for the HEAO-C case, long pulse lengths (0.5 ms) had to be employed, thus limiting the range resolution to relatively large values (75 km). Integration time was set at 20 sec for each data record. Such large space and time resolutions are not desirable for observations of effects comparable in size to a single pulse length, or to events changing on minute time scales. These resolutions were adequate for the HEAO-C observations since the Centaur exhaust cloud spanned 100's of km and the event lasted for several hours. However, since a typical chemical release cloud from a sounding rocket payload reaches an approximate maximum radius of $\sim$ 50 km, an improved spatial resolution would be required for such experiments.

An improvement in range resolution to 10-20 km would require 0.1 ms pulses. Unfortunately such short pulses unfavorably impact the S/N levels, and require a longer integration time to obtain usable spectra (i.e. ones from which reliable spectral parameters, N_e, T_e, T_i, V_d, and composition, can be obtained). The advantages of using an incoherent scatter radar as a diagnostic tool quickly deteriorate if the length of integration time needed approaches the time-scales of the event being monitored. In general, attempts to minimize spatial and temporal resolution values conflict with the simultaneous desire to maximize the information obtained from spectral analysis.

A further active experiment observed by the Millstone Hill radar was during the Spacelab-2 mission in 1985 when the Space Shuttle's OMS engines were used to generate an ionospheric hole above New England [Mendillo et al., 1987]. The magnitude of the Spacelab-2 electron density depletion was much smaller than the earlier (HEAO-C) rocket-induced hole because of the smaller shuttle engines and the relatively weak solar minimum ionosphere. A relatively long radar pulse length (0.3 ms) and 20 second integrations were used to maximize the power return to obtain accurate measurements of the electron density, thus determining the trade-off between power and spectral resolution.

During the same Spacelab-2 mission, an engine burn was conducted over the Arecibo Incoherent Scatter Radar Facility in Puerto Rico [Bernhardt et al., 1988]. In this experiment, the 305 m diameter Arecibo dish was able to provide 600 m spatial resolution, using shorter 0.004 ms pulse lengths, and 5.6 second integration data records. Clearly, the Arecibo radar owing to its great size, does not suffer from the same power/spectral resolution trade-off that the smaller Millstone Hill dish does. However, the Arecibo dish has greatly limited steerability, and is generally restricted to observations within 20° of zenith, a potential handicap for use in off-zenith active experiments. For smaller antennas, the lag-profile analysis techniques recently developed for the Millstone Hill radar will help in improving range and time resolution. A 15 km resolution is now possible, representing a significant improvement over the previous 40 km value [Holt et al., 1988]. Thus the trade-off between power return and spectral accuracy faced during the HEAO-C and Spacelab-2 experiments can be relaxed.

II.2. Incoherent Scatter Radar as an Ion Mass Spectrometer.

A problem unique to active experiments is that the composition of the observed ionospheric plasma is changed by the released species, and the radar is often faced with ions not usually present in the natural ionosphere. A spectral analysis program that is not expected to handle unusual ions will misinterpret the presence of those ions as changes in other parameters (i.e., temperature).

The IS spectrum for a mixture of ions is a superposition of the spectra for the individual ions, smoothed out by the Coulomb interactions (Moorcroft 1964). The presence of a mixture will be most clearly revealed in the spectral shape when there is a large difference in the ion masses.

The ions created in the HEAO-C and Spacelab-2 releases [OH^+ (17 amu), H_2O^+ (18 amu), and O_2^+ (32 amu)] were not notably different in mass from naturally occurring ionospheric ions [O_2^+ (32 amu), O^+ (16 amu)]. The effects of such ions on the shape of an IS

spectrum are small, and their presence is not easily inferred. However, some active experiments use heavy elements never found in the ionosphere, even under extreme circumstances. Over the years, a variety of experiments have been conducted using Ba (137 amu) releases, and a much smaller number using clouds of SF_6 (146 amu). The planned NICARE-1 and -2 experiments will release CF_3Br and $Ni(CO)_4$, which will produce the ions Br^- (80 amu) and $Ni(CO)_3^-$ (143 amu) [Bernhardt, 1987a].

To illustrate the effect of heavy positive ions on incoherent scatter spectra, a simulation of the spectrum associated with a barium plasma (Ba^+/e^-) in the F-region (O^+/e^-) has been conducted by Sultan et al. [1989]. The main effects are to pull the spectral wings in, and to make the peaks higher (Figure 1). The situation is analagous to the effect of H^+ on the spectrum of an O^+/e^- plasma, where the H^+ pulls the spectral wings outwards and lowers the peaks. In both instances two positive ions of very different masses are being mixed. For a given electron density, as the concentration of one ion is increased, the concentration of the other must decrease in order to keep the plasma electrically neutral. The change in spectral shape as the concentration of heavy positive ions increases is a diminishing of the spectral wings of the lighter ion, while the peaks of the heavier ion become more prominant. The total area under the spectral curve is constant since the background electron density is not changing.

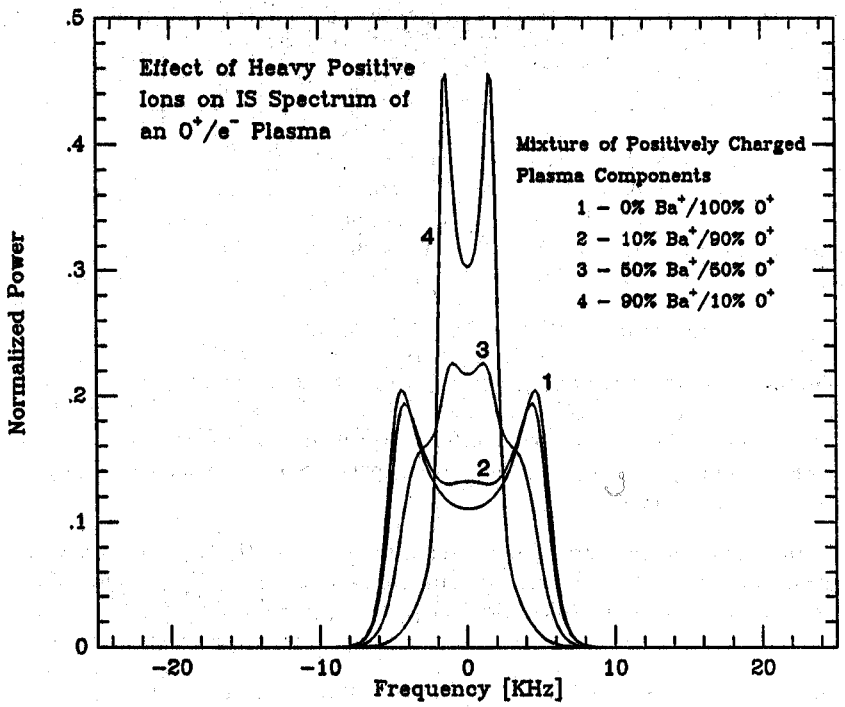

Figure 1. Theoretical incoherent scatter radar power spectra for different concentrations of heavy positive ions (Ba^+, 137 amu) on an O^+/e^- plasma ($T_e/T_i = 2.$). Curves 1 through 4 represent 0%, 10%, 50% and 90% Ba^+, respectively.

Figure 2 illustrates the effect of different concentrations of heavy negative ions (SF_6^-, 146 amu) on the IS spectrum of an O^+/e^- plasma. Such plasmas, containing both heavy negative, and lower-mass positive ions, were created during the NASA/Boston University SPINEX campaign through the release of SF_6 at F-region altitudes. SF_6, which has a high electron affinity, quickly attaches an ambient electron to itself ($SF_6 + e^- \longrightarrow SF_6^-$) creating a heavy, negatively charged ion. Since the newly formed plasma mixture must also be electrically neutral, the number of positively charged components must equal the number of negatively charged components, so that $N(O^+) = N(SF_6^-) + N(e^-)$. For the previous case of heavy positive ions, the charge neutrality relation was $N(O^+) + N(Ba^+) = N(e^-)$.

As was noted in Mendillo and Forbes (1982), the presence of heavy negative ions pulls the spectral wings outwards, and makes the shoulder features sharper and more peaked. An additional central hump is also added. The overall effect is similar to the spectral changes brought on by an increase in the T_e/T_i ratio (Figure 3), with the exception of the new central hump. This new peak, which actually appears to be two low frequency peaks very close to the transmitted radar beam frequency, has an additional mass dependency, and is more pronounced the heavier the ion is. The total area under the spectral curve does decrease in this case, since the total number of electrons available to scatter the radar beam has been reduced due to their conversion to the negatively charged ions.

If such spectral changes are taken into account by the radar analysis routine, an incoherent scatter radar can be used as a de facto mass spectrometer to track the spatial and temporal development of a heavy negative ion plasma cloud created during an active experiment. For a nighttime experiment, the overall strategy is to assume that the ambient temperature and composition of the background ionospheric plasma does not change over the short duration of the experiment, and that the new plasma from the ionized components of the chemical release quickly reaches temperature equlibrium. The temperature structure of the ionosphere is then fixed to a pre-event average, and the spectral analysis program is modified to recognize heavy negative ion effects. The analysis program will then view any spectral changes as being caused by changes in composition, and not due to changes in temperature. A program that does not take the presence of heavy negative ions into account will erroneously attribute the effect of the ions to a temperature change. Thus the ion mass spectrometer capabilities of an incoherent scatter radar can be exploited.

The presence of 10% or more SF_6^- has been successfully detected in the SPINEX-2 (1986) data set [Sultan et al, 1989]. Analysis of the SPINEX-1 (1984) and AFGL IMS (1983) SF_6 release data sets is underway. Incoherent Scatter Mass Spectrometry (ISMS) of heavy negative ions will be further tested during the NASA CRRES SF_6 (1990), and NASA/NRL NICARE releases of CF_3Br and $Ni(CO)_4$ (1989,1990). An incoherent scatter scan has yet to be performed on a heavy positive ion release, but several opportunities will occur during the CRRES experiments over Arecibo in 1991.

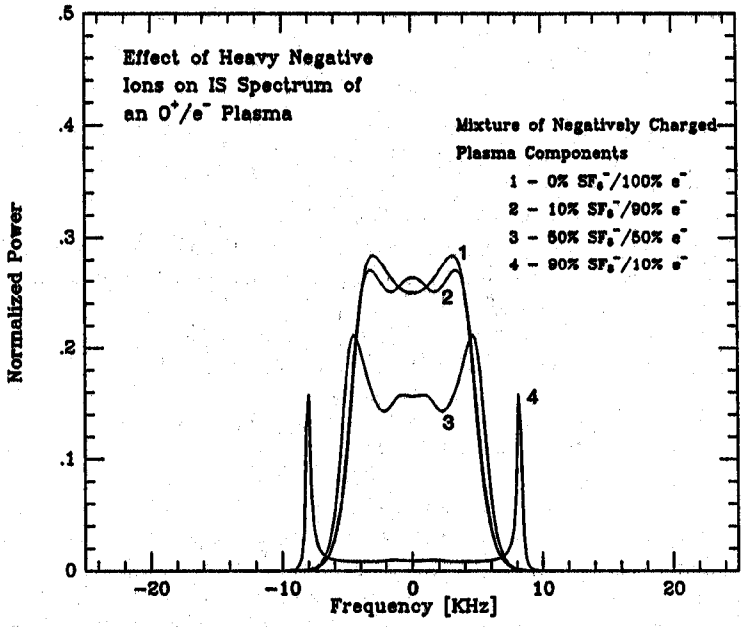

Figure 2. Theoretical incoherent scatter radar power spectra for different concentrations of heavy negative ions (SF_6^-, 146 amu) on an O^+/e^- plasma ($T_e/T_i = 1.$). Curves 1 through 4 represent 0%, 10%, 50% and 90% SF_6^-, respectively.

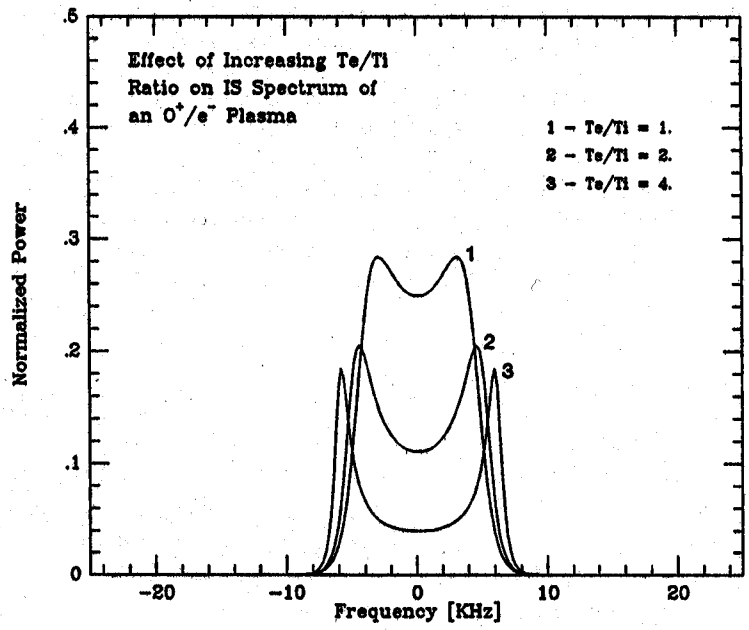

Figure 3. Theoretical incoherent scatter radar power spectra for a pure O^+/e plasma for different values of the T_e/T_i ratio. Curves 1 through 3 represent $T_e/T_i = 1.$, 2, and 4. respectively.

III. Low-Light-Level Optical Instrumentation Applied to Active Experiments

III.1. Background

Optical instrumentation using image intensifiers has been applied to a wide variety of geophysical and space plasma phenomena. A film-based image intensified system was first applied to ionospheric hole airglow studies [Mendillo and Baumgardner, 1982a] using a camera developed for aeronomic studies [Mendillo and Baumgardner, 1982b]. A CCD-based digital camera system was later developed [Baumgardner and Karandanis, 1984] and applied successfully to ionospheric modification studies [Mendillo et al., 1987]. Alternate CCD-based systems were developed and used in several ionospheric and magnetospheric chemical release experiments [Bernhardt et al., 1988, 1987b], and in ionospheric heating experiments [Bernhardt et al., 1989].

Each of the systems described in the references cited successfully addressed the fundamental issues faced by optical diagnostics devoted to active experiments: (1) weak signals at ambient atmospheric emission lines; (2) duty cycle concerns relating length of integration times and image storage times to the time scale of effects to be observed; (3) operational choices concerning dynamic range levels or image intensifier phosphor persistence ("afterglow") effects.

Fabry-Perot systems have been used extensively in aeronomic research, but only recently has the technique been applied to active experiments. A Fabry-Perot system used in high altitude barium release observations was described by Mende and Harris (1982). The AMPTE program of chemical releases included Fabry-Perot measurements of barium released into the geomagnetic tail [Mende et al., 1989], as well as into the solar wind [Rees et al., 1986]. The Doppler Imaging System (DIS) used in the latter case is described in Rees et al., (1984). Opportunities to apply these techniques to releases in the thermosphere-ionosphere system will occur during the NASA CRRES missions scheduled for 1990-91.

In the following sections, brief descriptions will be given of two new instruments that are well suited for observations of active experiments in the ionosphere: a low-light-imager and a meridional imaging spectrograph.

III.2. The CEDAR Imaging System.

As part of a U.S. National Science Foundation initiative in atmospheric sciences, the CEDAR ("Coupling, Energetics and Dynamics of Atmospheric Regions") Program has sought to establish instrumentation and programmatic upgrades in all areas of aeronomic research (CEDAR, 1986). One of the core instruments developed for optical diagnostics was a state-of-the-art imaging system. The CEDAR Class-I imager is expected to advance ground-based capabilities for upper atmospheric research in two fundamental ways: (1) provide high quality, fully-calibrated, all-sky images at multiple wavelengths for research in optical aeronomy, (2) provide a facility class instrument to operate in campaign mode in conjunction with simultaneous observations by incoherent scatter radar, Fabry-Perot, LIDAR, and spectrograph systems, as well as other diagnostics clustered for a given set of geophysical research objectives.

The CEDAR Imager became operational on 1 September 1989 and is located on the Haystack Observatory complex in Westford, MA (USA). It is used in conjunction with the Millstone Hill radar and optical and radio facilities in the area. Typical results to be expected from such a cluster of instruments observing geophysical effects are treated in Mendillo et al., (1987). The imaging system itself may be readily applied to active experiments, as shown in Baumgardner and Karandanis (1984) for an earlier generation system.

Figure 4 gives a schematic of the CEDAR imager. When operated in the all-sky mode, light from 2π steradians is imaged onto the field lens where it is re-directed into the collimator. After the collimator, the light is in parallel bundles 100mm in diameter with a maximum angle of any ray to the optical axis of 4.5°. This small angle allows the use of interference filters with band passes of $\sim$ 12Å HPFW. After passing through the filter the light is re-imaged at f/1 onto the photocathode of the intensified CCD. This detector is housed in a refrigerated housing and is kept at near -40°C to reduce its dark signal and thus allow the camera to integrate for 1 minute before the dark signal becomes significant. Figure 5 shows the sensitivity curves for the CEDAR detector and Figure 6 shows the performance of the detector under typical nightglow conditions.

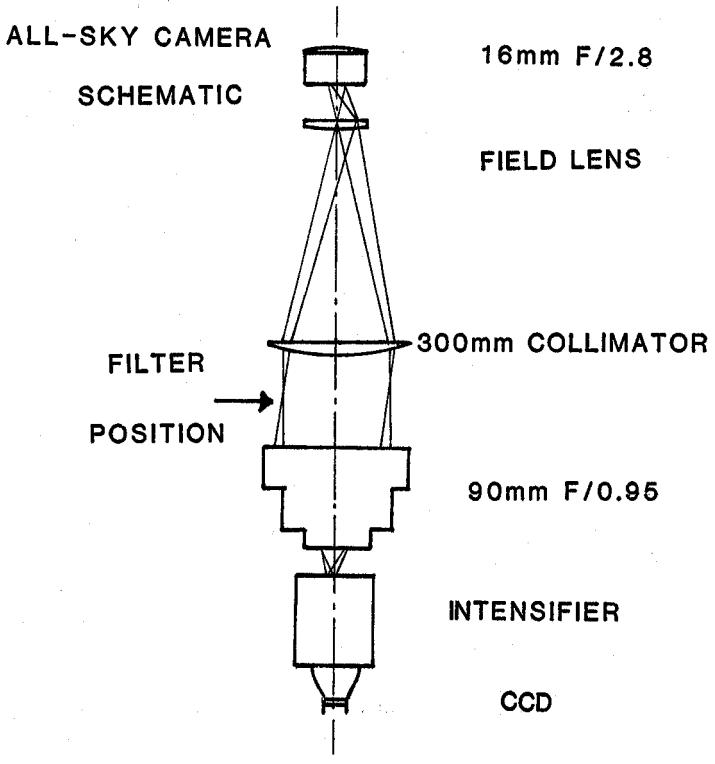

Figure 4. Schematic Diagram of CEDAR Imager.

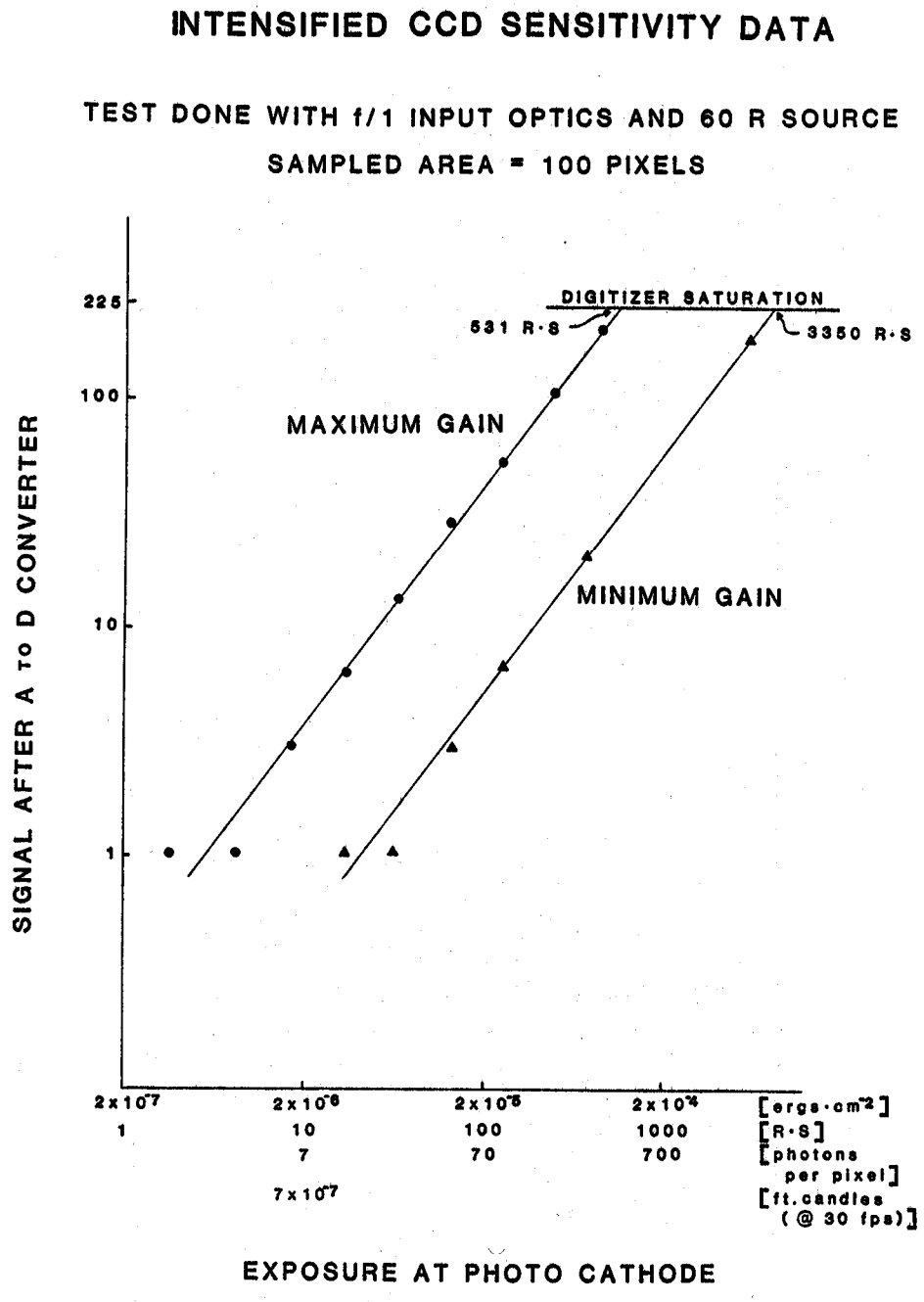

Figure 5. Sensitivity curves for CEDAR Detector.

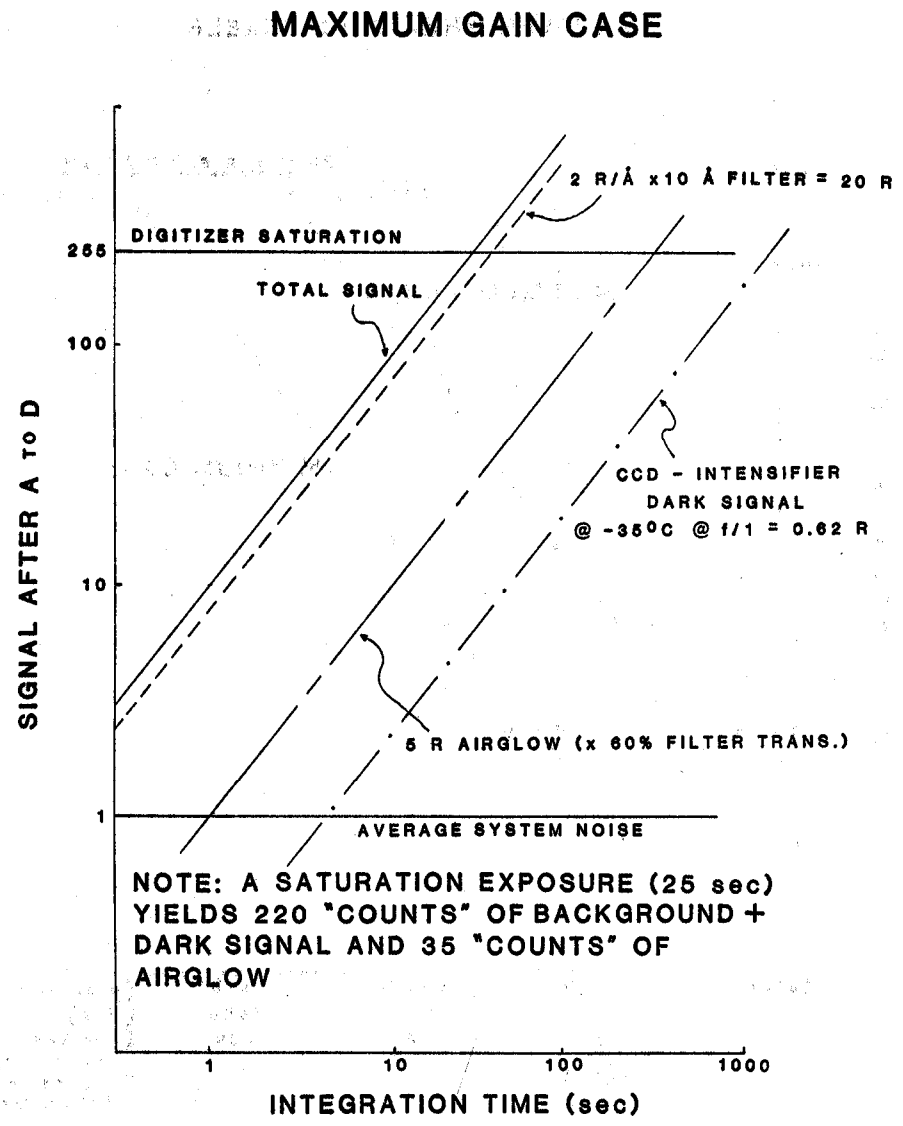

Figure 6. Performance curves of CEDAR detector under typical nightglow conditions.

III.3. Meridional Imaging Spectrograph

In many active experiments there are reasons to search for optical emissions over extended spatial and spectral domains. Investigations of geophysical structures (e.g., aurora) often also require simultaneous multi-wavelength coverage across extended features. To address these needs, a new meridional spectrograph was designed and tested (Baumgardner, 1989). Figure 7 gives a schematic of the prototype system. Its design is very similar to the CEDAR imager except that a reflection grating is used in place of the interference filter, and a slit is placed on the plano surface of the field lens. At the detector, the image of the slit at each wavelength has 360 spatial resolution elements corresponding to 180° field of view of the all-sky lens. The projected slit width is $\sim 1°$. In the dispersion directon there are 488 pixels, with the instrumental profile covering $\sim$ 10Å and a spectral range of 2000Å for any given grating position.

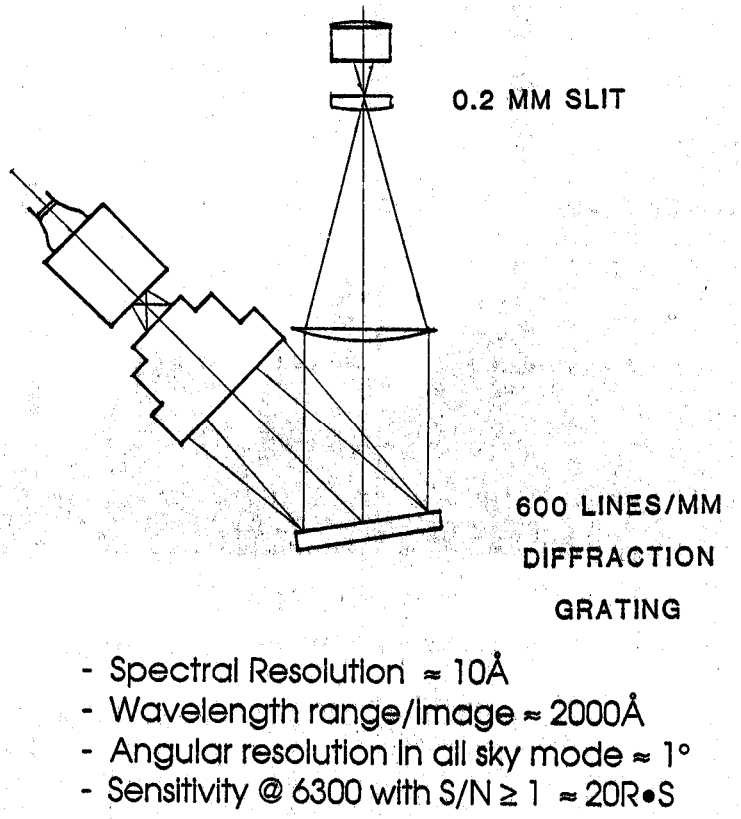

Figure 7. Schematic diagram of Meridional Spectrograph.

Figure 8, gives an example of a wavelength slice through a 30 second integration of nightglow from ~ 6300Å to 8300Å. The photocathode wavelength sensitivity curve has not been removed and is responsible for the downward slope of the spectrum toward the red end.

Since each integration can be saved on a WORM (Write Once Read Many) optical disk drive and each spectra contains spatial information along the slit, an image for each wavelength can be reconstructed showing space, time and intensity. Through a different choice of front end optics, the field of view can also be reduced from all-sky (meridional) to a narrow field mode more appropriate for small scale active experiments.

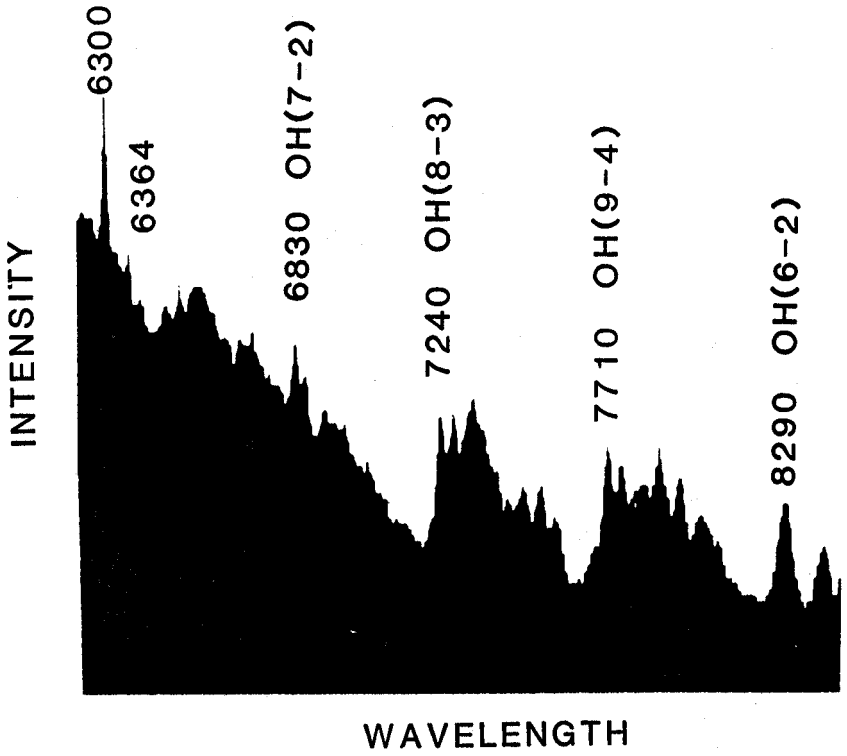

Figure 8. Zenith slice of spectrum taken with Meridional Spectrograph.

As a final point, it should be emphasized that the acquisition of digital images using CCD technology leads to a scale of data analysis work not encountered with earlier film-based systems. The advantages of working with digital images outweigh their drawbacks, but significant resources (personnel, hardware and software) are required to extract the full scientific yield from such systems. In Figure 9, we present in schematic form the data acquisition and processing system required for timely reduction and analysis of both CEDAR imager and meridional spectrograph images.

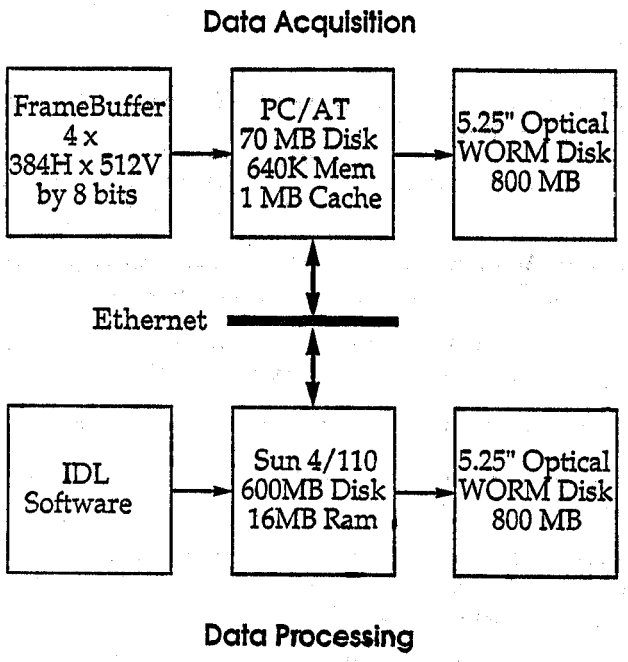

Figure 9. Data acquisition and processing schematic for CEDAR-type detector.

Acknowledgements. This work was supported, in part, by NASA grants, # NAGW-1629, and ATM# NAS8-36324, and by NSF grant, # ATM-8709487. We are grateful to Professor William Oliver for suggestions and discussions covering the incoherent scatter radar material, and to Ms. Kathryn Collins for her careful preparation of the typescript.

References

Baumgardner, J., and S. Karandanis, CCD System Using Video Graphics Controller, *Electronic Imaging, 3*, 28, 1984

Baumgardner, J., A Meridional Spectrograph for Aeronomic Studies, *EOS, 70*, 404, 1989.

Bernhardt, P.A., A Critical Comparison of Ionospheric Deplection Chemicals, *J. Geophys. Res., 92*, 4617, 1987a.

Bernhardt, P.A., Roussel-Dupre, R.A., Pongratz. M.B., Haerendel, G., Valenzuela, A., Gurnett, D.A., and R.R. Anderson, Observations and Theory of the AMPTE Magnetotail Barium Releases, *J. Geophys, Res., 92*, 5777, 1987b.

Bernhardt, P.A., Tepley, C.A., and L.M. Duncan, Airglow Enhancements Associated with Plasma Cavities Formed During Ionospheric Heating Experiments, *J. Geophys. Res., 94*, 9071, 1989.

Bernhardt, P.A., Kashiwa, B.A., Tepley, C.A., and S.T. Noble, Spacelab-2 Upper Atmo-

spheric Modification Experiment Over Arecibo, 1, Neutral Gas Dynamics, *Astrophys. Lett. Comm., 27*, 169, 1988.

Brenning, N. (editor), Critical Ionization Velocity Phenomena, *Adv. Space Res., 10,* (8), 1989.

Burke, W.R. (compiler), Active Experiments in Space, *Proceedings of Symposium at Alpback*, Austria, 24-28 May, 1983, European Space Agency Report ESA-SP-195, Paris, France.

CEDAR, Coupling, Energetics and Dynamics of Atmospheric Regions, Vol. 1. Overview, Aeronomy Program, Nat. Sci. Found., Washington, DC, USA 1986.

Evans J.V., High-Power Radar Studies of the Ionosphere. *Proc. IEEE, 63,* 1636, 1975.

Evans J.V., Theory and Practice of Ionosphere Study by Thomson Scatter Radar. *Proc. IEEE, 57,* 496, 1969.

Foppl, H., Haerendel, G. Haser, L., Loidl, J., Lutjens, P., Lust, R., Meltzner, F., Mayer, B., Neuss, H., and E.R. Rieger, Artificial Strontium and Barium Clouds in the Upper Atmosphere, *Planet. Space Sci., 15*, 357, 1967

Haerendel, G. and M. Mendillo (editors), Active Experiments, *Adv. Space Res., 8*, (1), 1988.

Haerendel, G., Modification of Ionized Media by Chemical Substances — A Review of Physical Processes, AGARD Conference Proceedings No. 192, (H.J. Albrecht, ed.) 13-1, AGARD (Bruxelles), 1976

Heppner, J.P., Stolarik, J.D., and E.M. Wescott, Electric Field Measurements and the Identification of Currents Causing Magnetic Disturbances in the Polar Cap, *J. Geophys. Res., 76*, 6028, 1971.

Holt J.M., Rhoda D.A., Tetenbaum D. and VanEyken A.P., A New Technique for the analysis of Incoherent Scatter Lag Profile Measurements. Presentation at COSPAR XXVII, Helsinki, 1988.

Mende, S.B., Swenson, G.R., Geller, S.P., Doolittle, J.H., Harendel, G., Valenzuela, A. and O.H. Bauer, Dynamics of a Barium Release in the Magnetosphere Tail, *J. Geophys. Res.,* (in press), 1989.

Mende. S.B. and S.E. Harris, Measure of the Line of Sight Velocity of High Altitude Barium Clouds: A Technique, *Applied Optics, 21*, 3348, 1982.

Mendillo, M. (editor), Active Experiments in Space, *Adv. Space Res., 10*, (8), 1989.

Mendillo, M., Ionospheric Holes: A Review of Theory and Recent Observations, *Adv. Space Res., 8*, 51, 1988.

Mendillo, M., and J. Baumgardner, Optical Signature of an Ionospheric Hole, *Geophys. Res. Lett., 9*, 215, 1982.

Mendillo, M., and J. Baumgardner, Airglow Characteristics of Equatorial Plasma Depletions, *J. Geophys. Res., 87*, 7641, 1982b.

Mendillo, M., Baumgardner, J., Aarons, J., Foster, J., and J. Klobuchar, Coordinated Optical and Radio Studies of Ionospheric Disturbances: Initial Results from Millstone Hill, *Annales Geophysicae, 5A*, 543, 1987.

Mendillo M., Baumgardner J., Allen D.P., Foster J., Holt J., Ellis G.R.A., Klekociuk A., Reber G., Spacelab-2 Plasma Depletion Experiments for Ionospheric and Radio Astronomical Studies. *Science, 238,* 1260, 1987.

Mendillo M. and Forbes J., Theory and Observation of a Dynamically Evolving Negative Ion Plasma. *J. Geophys. Res., 87,* 8273, 1982.

Moorcroft D.R., On the Determination of Temperature and Ionic Composition by Electron Backscattering from the Ionosphere and Magnetosphere. *J. Geophys. Res., 69,* 955, 1964.

Rees, D., Greenaway, A.H., Gordon, R., McWhirter, I., Charleton, P.J. and A. Steen, The Doppler Imaging System: Initial Observations of the Auroral Thermosphere, *Planet. Space Sci., 32*, 273, 1984.

Rees, D., Hallinan, T.J., Stenback-Nielsen, H.C., Mendillo, M., and J. Baumgardner, Optical Observations of the AMPTE Artificial Comet From the Northern Hemisphere, *Nature, 320,* 704, 1986.

Rosenbluth M.N., Rostoker N., Scattering of Electromagnetic Waves by a Non-Equilibrium Plasma. *Phys. Fluids, 5,* 776, 1962.

Stenbaek-Nielsen, H.C., Hallinan, T.J., and E.M. Wescott, Acceleration of Barium Ions Near 8000 km Above an Aurora, *J. Geophys. Res., 84*, 10788, 1984

Sultan P.J., Mendillo M., Oliver W.L., Holt J., Detecting Heavy Negative Ions With an Incoherent Scatter Radar During Active Experiments, *EOS*, Nov. 1989.

Wand R.H. and Mendillo M., Incoherent Scatter Observations of an Artificially Modified Ionosphere. *J. Geophys. Res., 89,* 203, 1984.

Wescott, E.M., Stenbaek-Nielsen, H.C., Hallinan, T., Foppl, H. and A. Valenzuela, Star of Condor: A Strontium Critical Velocity Experiment, Peru, 1983, *J. Geophys. Res., 91*, 9933, 1986.